Solid State Communications 175-176 (2013) 90–100

Contents lists available at ScienceDirect

Solid State Communications

journal homepage: www.elsevier.com/locate/ssc

Modeling electronic properties and quantum transport in doped and defective graphene

A.R. Botello-Méndez *, A. Lherbier, J.-C. Charlier

Université catholique de Louvain (UCL), Institute of Condensed Matter and Nanosciences (IMCN), Chemin des étoiles 8, 1348 Louvain-la-Neuve, Belgium

ARTICLE INFO

Article history:
Received 24 April 2013
Received in revised form
23 August 2013
Accepted 26 August 2013
Communicated by Toshiaki Enoki
Available online 8 September 2013

Keywords:
A. Graphene
D. Electronic structure
D. Electronic transport
E. Numerical simulations

ABSTRACT

The outstanding transport properties of graphene drastically depend on the details of its atomic structure. Thus, modifying the carbon hexagonal network at the atomic level in the form of point defects (chemical dopants, structural modifications) or extended defects (grain boundaries, extended lines of defects) is of paramount importance for the complete understanding of experimental transport measurements on "real" graphene samples. Furthermore, it is crucial to deeply scrutinize the effect of a specific defect on the electronic structure of graphene, because controlled defect introduction may be used to tune the transport properties of graphene in a desired direction for specific applications. In this review, the landscape of defects and their importance in both the electronic structure and the transport properties of graphene are presented using *ab initio* and *tight-binding* simulations.

1. Introduction

The history of the study of defects in sp^2 carbon-based systems is as rich and as old as the elucidation of the crystal structure of graphite in the first decades of the 20th century [1–4]. It began with the synthesis of different stacking orders and random stacking in graphite. For some decades, research on this subject was dominated by the effects that interstitials could introduce into graphite, leading to the field of graphite intercalation compounds, where staggering is a clear example of controlled introduction of defects in order to change the properties of this rich compound [5].

The advent of nanoscale carbon, from fullerenes to nanotubes, graphene, and even carbon chains, has triggered renewed concerns on the effect of defects on sp^2 carbon. The interest consists either in understanding sources of detriment for electronic, thermal or optical characteristics, or tuning and tailoring properties on demand for specific applications.

In sp^2 carbon systems, defects are localized either in the interplanar region (e.g. graphite intercalation compounds, nested fullerenes or multiwall nanotubes), or directly in the hexagonal planar network. Within this plane, it is common to classify defects as intrinsic and extrinsic. In the former, the lattice order is perturbed without the addition of foreign atoms. In the latter, atom impurities are responsible for the deviation from perfect crystals. Yet, when looking at the electronic and transport properties of materials, it is often useful to classify defects by their extension in real-space.

In this work, we present a general overview of the effect that different kinds of in-plane defects have on the electronic and transport properties of graphene using state-of-the-art simulations. The objective is to present a general picture of the information gathered from present standard modeling techniques which are considered relevant for applications within a framework of what is possible experimentally. A broad view can only be obtained through a multi-scale approach for systems scaling from a few nanometers to few micrometers. Such an endeavor must include studies carried out using first-principles calculations, semi-empirical *tight-binding* models, and different kinds of transport approaches, which are all within the scope of this review.

The first section presents a brief description of the properties of graphene with a few references to recent scientific reviews. Then, an overview of point defects both intrinsic and extrinsic is presented, concluded with a subsection on the typical effects that these defects have on graphene systems at different scales. Afterwards, the effect of extended defects including grain boundaries and extended lines of defects is surveyed. Finally, the extreme case of highly defective or quasi-amorphous graphene is examined, after which conclusions are drawn. For the sake of legibility, the methods used on this and other works presented in this review are briefly presented in the last section.

2. Pristine graphene

An ideal graphene sheet is a two-dimensional (2D) carbon allotrope composed by two triangular sublattices forming a hexagonal network, the so-called honeycomb lattice. Such a 2D

* Corresponding author. Tel.: +32 10478566.
E-mail address: andres.botello@uclouvain.be (A.R. Botello-Méndez).

0038-1098/$ - see front matter © 2013 Elsevier Ltd. All rights reserved.
http://dx.doi.org/10.1016/j.ssc.2013.08.029

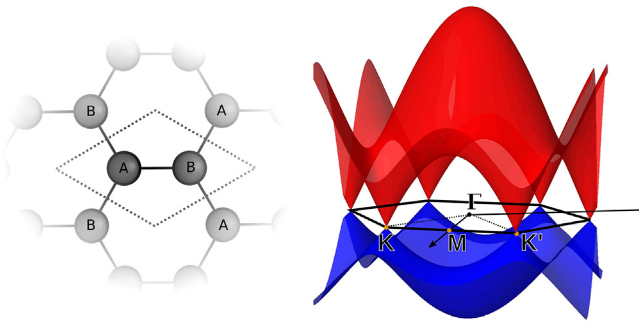

Fig. 1. (Color online) Crystal structure of graphene illustrating the different sublattice sites, and π–π^* tight binding electronic structure showing the Dirac cones at the corners of the Brillouin zone.

sp^2 carbon system is a zero band gap semiconductor with the peculiarity that its valence and conduction bands both exhibit a conical shape meeting at the corners of the Brillouin zone and exactly at the Fermi level (see Fig. 1). Thus, the Fermi surface is reduced to two non-equivalent points (K and K') around which the electronic dispersion is linear. That is, $E(k) = \pm v_F \hbar k$, where v_F is the Fermi velocity, and k is the momentum measured with respect to K or K'. Such a particular band structure gives rise to outstanding electronic and transport properties responsible for the large attention that graphene has received for its potential applications.

Values for the mobility of charge carriers up to the order of $10^6\ \mathrm{cm^2\ V^{-1}\ s^{-1}}$ have been reported for suspended graphene [6]. Since, the density of states of pure graphene vanishes at the Fermi level, the electrical conductivity is expected to vanish as well. However, various experiments suggested that there is always a minimum of conductivity, related to the quantum of resistivity [7]. In addition, the linear dispersion of graphene electronic spectrum is analogous to the solution of a 2D massless Dirac Hamiltonian $H_K = v_F \boldsymbol{\sigma} \cdot \boldsymbol{p}$ close to K, and $H_{K'} = -H_K$, whose solutions are referred to as the K and K' valleys. The operators $\boldsymbol{\sigma}$ and $\boldsymbol{p}$ are the Pauli matrices $\boldsymbol{\sigma} = (\sigma_x, \sigma_y)$, and the momentum operator, respectively. However, for the case of graphene, $\boldsymbol{\sigma}$ is not an operator on the electronic spin, but rather corresponds to the two degenerate sublattices, and hence this spinorial component of the wave function reflects the bipartite nature of the graphene honeycomb lattice. It is commonly referred to as the *pseudospin*. An interesting consequence is summarized by the helicity operator $\hat{h} = \boldsymbol{\sigma} \cdot \boldsymbol{p}/p$ which expresses the fact that the pseudospin is either parallel or antiparallel to the momentum, and thus has eigenvalues of ± 1, and charge carriers (holes and electrons) have an opposite helicity (or chirality) in opposite valleys [6,7].

3. Point defects

3.1. Dopants

The idea of doping graphene follows, at least in its beginnings, the well established concept of tuning the electronic properties of an otherwise pure material by introducing impurities in a controlled way. Foreign atoms add extra electrons (negative charge n) or holes (positive charge p) to the host material, thus changing its electronic behavior. The idea of doping and the related theories have played an important role in the development of logical unipolar field effect transistors (FETs) and in the concept of p–n junctions which has been a corner stone in the realization of analogical bipolar transistors.

For the case of graphene, the addition of extra holes and electrons is usually envisaged with boron and nitrogen atoms, respectively. Since only few studies are dedicated to graphene doped with other atoms, and are mostly hypothetical, this work focuses on nitrogen (N) and boron (B) doped graphene, which have been synthesized by several methods [8–26], and are representative examples of the change of the electronic properties of graphene through chemical impurities.

It is noteworthy that in contrast to classic semiconductors, dopants in 2D graphene are exposed in the surface, changing dramatically the chemical properties of graphene. For this reason, doped graphene has found potential applications in fields distinct from electronics. Doped graphene has been proposed as an active material in electrocatalysis for oxygen reduction [27–34], methanol oxidation [35], field emission [36,37], ultracapacitors [38], catalyst for hydrogen dissociative adsorption for fuel cells [39], sensors [40,41], lithium batteries [42], and hydrogen storage [43,44].

In a 2D (as well as in a 1D) material, the effect of the incorporation of extrinsic defects on its electronic properties is expected to have a significant dependence on the atomic details of the impurity configuration. This is a consequence of the low dimensionality and electron confinement. It is therefore crucial to obtain an atomic scale characterization of the material. Several experimental studies have gathered evidence on the incorporation of nitrogen into the graphene lattice [18,26,45] using scanning tunneling microscopy and spectroscopy (STM/STS) images and spectra. Joucken and coworkers showed that the exposure of graphene to a nitrogen plasma flux after synthesis leads to a homogeneous distribution of substitutional atoms [45]. However, when a nitrogen source is introduced during the CVD growth of graphene, the nitrogen incorporation exhibits a preferential accommodation within one of the two triangular sublattices that compose the honeycomb lattice [18,26]. This wayward incorporation of nitrogen atoms into graphene is presently not hitherto understood. However, calculations point towards long range interaction as a possible cause of such a sublattice preference [26,46].

Nevertheless, an important step towards the understanding of the effect of the incorporation of nitrogen atoms into the graphene lattice has been achieved through STM and STS imaging and simulation [18,26,45,46]. These studies have demonstrated that the atomic identification of defects in graphene is not trivial, and *ab initio* simulation is an important tool to analyze and understand the experimental data (see Fig. 2).

In general, STM image simulation carried out under the Tersoff–Hamann [47] approximation is good enough for screening possible atomic configurations of the foreign atoms. Several groups have reported several simulated STM images for different atomic configurations of dopants (mainly nitrogen and boron) into graphene [26,48,49]. However, the simulated images often depend on the specific window of energy for the integration of the local density of states (LDOS) used. This energy window is related to the bias used for experimental imaging. As representative examples, Fig. 2 shows the atomic structure and simulated STM images of different nitrogen and boron configurations. The STM image is obtained from the integration of the LDOS within a window of energy starting from the Dirac point (or its reminiscence) to the peaks on the density of states (DOS) characteristic of the localized states related to the defect (shaded regions of the DOS in Fig. 2).

Unfortunately, it is not always easy to make a straight-forward correlation between experimental and simulated STM images. For instance, substrate doping or charge puddles often frustrate the determination of the exact position of the Dirac point or its reminiscence. For this reason, it is desirable to compare not only simulated STM images, but also STS spectra, which is related to the projected density of states (PDOS) around a given atom. Such a comparison renders a more reliable identification of a dopant in graphene [26]. In addition, information related to the position of the resonant states induced by the dopant is also provided. The latter are extremely relevant for the transport properties, specially at low dimensions.

3.2. Structural defects

Structural modification at the atomic level of the graphene lattice is also expected to strongly impact its ideal electronic properties which directly arise from its honeycomb structure. In this respect, topological defects, defined as the introduction of non-hexagonal rings in the carbon lattice while preserving the three-fold connectivity of each carbon atom, play a very important role in graphene and related nanostructures [50,51]. From a structural point of view, the introduction of pentagons in an otherwise perfect honeycomb lattice leads to a deficit of 60°, inducing positive curvature. In contrast, a heptagonal ring introduces an excess of 60°, thus creating a saddle point in the honeycomb lattice. Pentagon–heptagon pairs can thus preserve the planarity of graphene. It is the case for the Stone–Thrower–Wales (S–T–W) defect [52,53] sometimes also called 55–77 defect which follows from the 90° rotation of a single carbon–carbon bond (see Fig. 3). In fact, the creation of large planar domains composed only of pentagons and heptagons, instead of hexagons is indeed possible and are referred to as pentaheptides structures [54]. More exotic planar structures can also be obtained by mixing the three kinds of carbon rings (pentagons, hexagons, and heptagons) and are referred to as haeckelites [55].

Among the various possible structural defects in graphene, a particular attention is devoted to carbon vacancies. These are easily produced during the synthesis of a graphene layer and have indeed been observed frequently. It is noteworthy that if the number of vacancies is odd, there will be dangling bonds that make the structure highly reactive and unstable. The possible routes for the stabilization of these structures are migration and fusion with another odd number vacancy [56], binding with the underneath substrate [57], or impurities such as molecules or atoms. Nevertheless, single vacancies induced by ion irradiation have revealed that lattice defects can be considered as a potential source of intervalley scattering [58] and zero energy modes

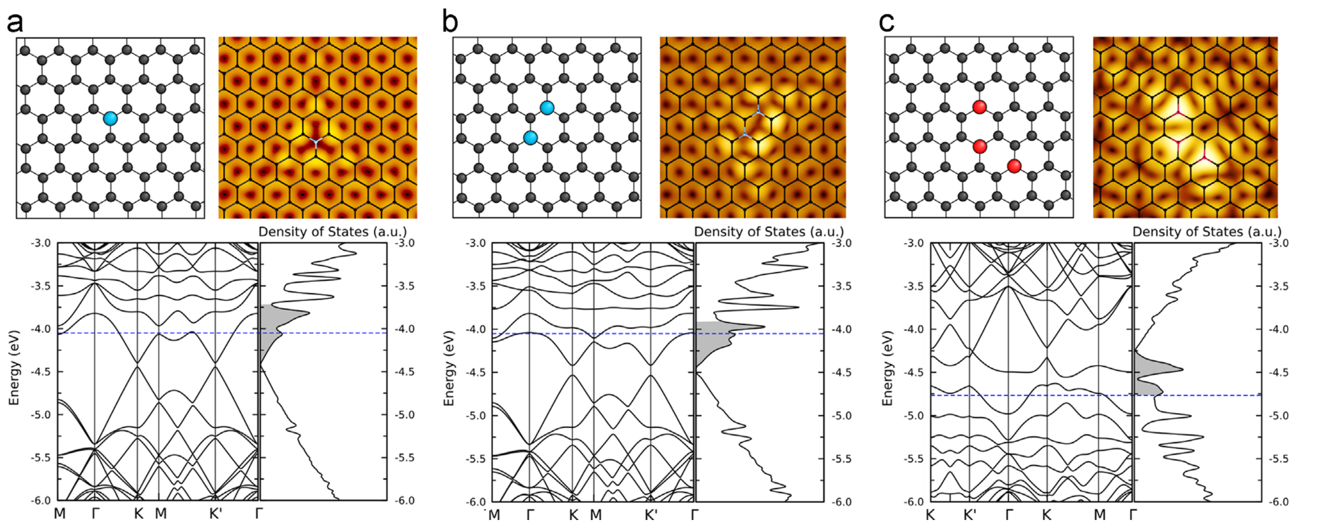

Fig. 2. (Color online) Modeling the effect of dopants in graphene. Atomic geometries, simulated STM images and electronic structure of (a) single substitutional N doping, (b) double substitution N doping and (c) triple substitution B doping. The simulated STM images are generated by integrating the shaded region of the density of states (see text). Fermi energy is indicated by a horizontal blue dashed line.

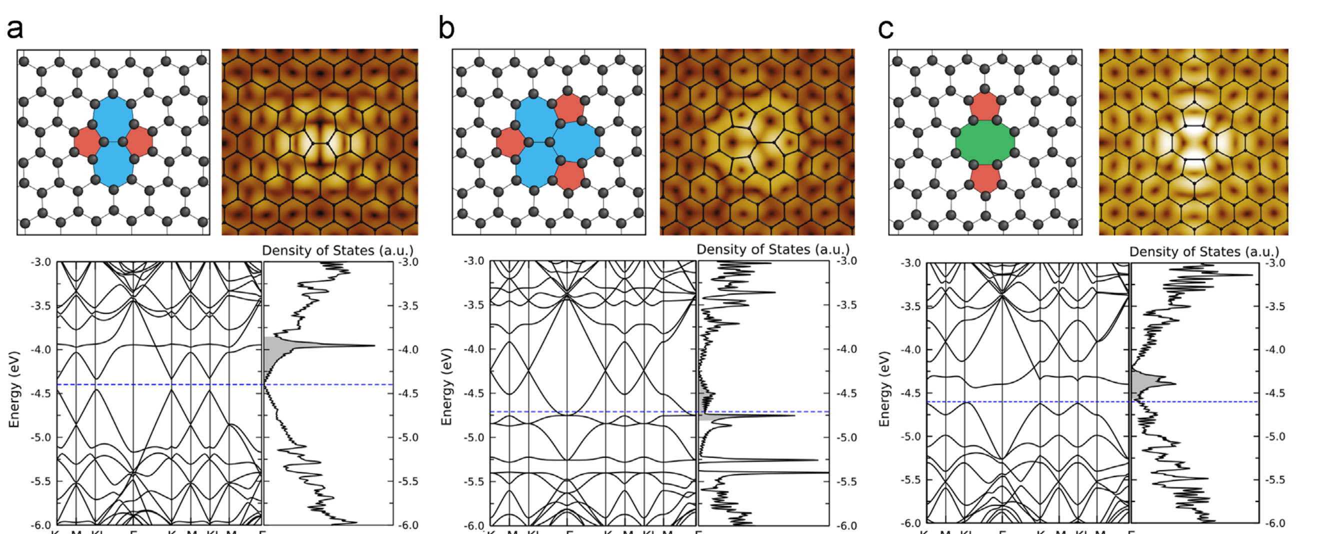

Fig. 3. (Color online) Modeling the effect of structural defects in graphene. Atomic geometries, simulated STM images, and electronic structures of (a) Stone–Thrower–Wales (S–T–W) defect, (b) triple pentagon–triple heptagon (t5t7) and (c) pentagon–octagon–pentagon (5–8–5). The simulated STM images are generated by integrating the shaded region of the density of states (see text). Fermi energy is indicated by a horizontal blue dashed line.

[59–61]. In addition, odd vacancies exhibit local moments which interact with electrons through the Kondo effect [62]. Even number vacancies can be reconstructed or healed in order to preserve the carbon–carbon connectivity. For instance a double vacancy, also called the divacancy, can be reconstructed in various geometries following the rotation of carbon–carbon bonds [63]. The known configurations of divacancies in graphene are the t5t7 (or 555–777), the q5–6–q7 (or 5555–6–7777), and the 5–8–5, where the numbers specify the various carbon membered rings (pentagons, hexagons, heptagons, or octagons) composing each defect. In contrast to odd vacancies presenting dangling bonds, even vacancies are not expected to exhibit a local magnetic moment. The atomic geometry, and the corresponding electronic structure, i.e. the band structure and the DOS, of a S–T–W defect, a t5t7 divacancy and, a 5–8–5 divacancy are displayed in Fig. 3a–c, respectively. Although the band structures of S–T–W defect and 5–8–5 divacancy seem to show a band gap in the electronic structure, the DOS unambiguously indicates the absence of a band gap. To obtain the band crossing, another path in the Brillouin zone has to be examined (see for instance [64,65]). Computed STM images for each of these structural defects are also presented in Fig. 3, which can be compared with experimental STM images [66,67]. As mentioned in the previous subsection, STM images correspond to the integration of the LDOS in a given range of energies (see shaded region in the DOS panels) which has been chosen to include the main resonant energy peak in the vicinity of the Fermi level. The exact position of these resonant energy peaks with regards to the Dirac point constitutes a fingerprint of each defect. Thus, in addition to the STM image, the STS spectra exhibiting such resonant peaks can serve as relevant characterization tools of point defects.

3.3. Transport with point defects

A comprehensive understanding of the effect of point-defect impurities on the transport properties of graphene and related systems requires a multiscale approach. Each scale determines the potential applications of the system in interest. In the following section, the effect of point defects on the transport properties on graphene systems is illustrated with the example of nitrogen doping.

At the bottom of the scale is the scattering of a single point defect on a graphene nanoribbon of relatively small lateral size (ca. 1 nm), where the effect is found to be quite relevant. Indeed, the doping of nanoribbons has been the subject of intensive research, since they are promising candidates for a plethora of nanoscale devices, such as sensors and electrochemical applications [68]. In these systems, the shape of the edges determine the electronic structure of the pristine material, and in particular the appearance and size of a band gap [69]. Due to the size of the system and the consequent ballistic regime, the Landauer–Buttiker formalism (see Section 7) is appropriate for this specific investigation. Regardless of the exact value of the gap, the introduction of a point defect yields to localized states which result in backscattering at specific resonant energies. For instance, Fig. 4a depicts an armchair nanoribbon of width ca. 2 nm, with a N impurity. A drop in transmission is observed at a resonant energy which depends on the exact position of the N-dopant with respect to the edges [70,71]. This drop can be as dramatic as the total suppression of the transmission channel, as it is illustrated for the case of the N-dopant located close to the edge (see Fig. 4a black curve).

As the size of the system increases to ca. 10 nm, the effect of a single point defect becomes negligible. Instead, the relevant scenario is a random distribution of impurities with a given concentration (see Fig. 4b). In this case, not only does the concentration play a role, but also the length of the channel, and the spatial distribution of dopants [72]. Following from the preferential sublattice doping observed experimentally [18,26], Fig. 4b shows the average quantum conductance of a 15 nm width nanoribbon of a random distribution of N dopants in a single sublattice (AA) in a ca. 30 nm long channel, and that of a random distribution of N dopants in both sublattices (AB). The inset in Fig. 4b shows the effect of the length of the AA N-doped channel on the transmission of carriers. The first plateau of conductance (holes: $E=-0.07$ eV; electrons: $E=+0.07$ eV) exhibits an increasing asymmetry as the length increases and the localization for holes becomes evident.

As the scale increases, edges and contacts become negligible, and a 2D treatment of the system is more adequate. Therefore, the use of the real-space order-N Kubo–Greenwood approach (see Section 7) is meaningful, and transport properties of large 2D graphene planes ($\sim 250\times 250$ nm^2 containing about 2.4 millions of atoms) with point defects can be addressed. In particular, graphene doped with

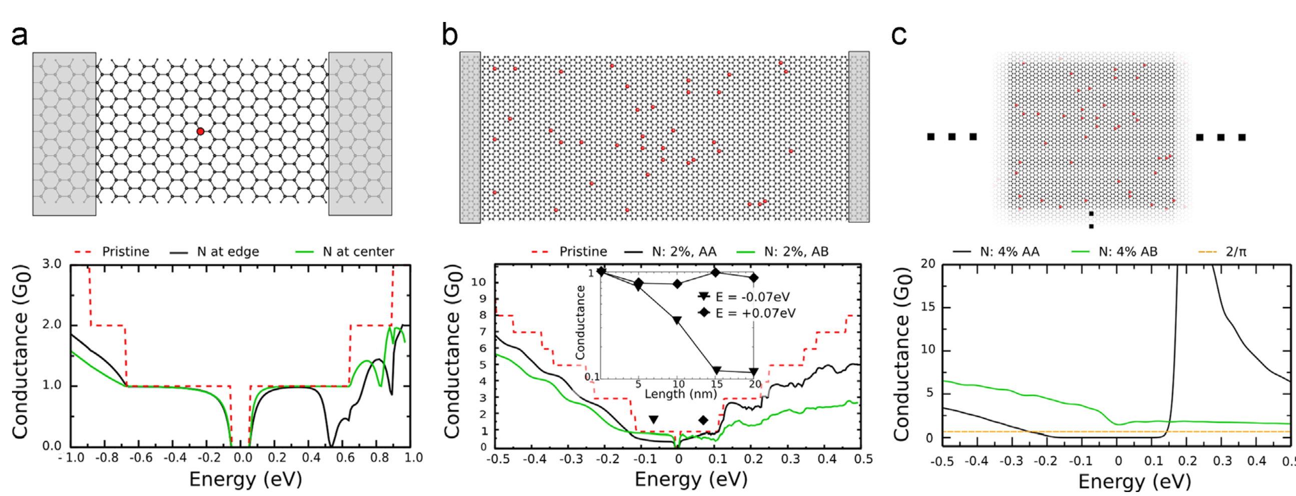

Fig. 4. (Color online) Modeling N-doping concentration in graphene at different scales: (a) a single N defect in a 1D nanoribbon of width ca. 2 nm, (b) random distribution of 2% N doping on a ca. 15 nm width nanoribbon, (c) random distribution of 4% N doping in a micrometer scale graphene plane. Their corresponding quantum conductance ($G_0 = 2e^2/h$) is illustrated in the panels below. In (a), the resonant state associated with the impurity depends on its exact position, e.g. at the center versus close to the edge, inducing localized scattering states in the conductance. In (b), the scattering effect is more homogeneous, and the effect of the distribution of the dopants in only one sublattice (AA) or on both sublattices (AB) is found to be important. The inset shows the conductance for holes (triangles) and electrons (diamonds) as a function of the length of the AA N-doped channel. In (c) a gap of ca. 340 meV is found to be induced in the case of a distribution in only one sublattice (AA). In addition, a high asymmetry between the electrons and holes is predicted.

different configurations and concentration of nitrogen impurities were investigated (see Figs. 4c and 5). First, a random distribution of nitrogen dopants within both sublattices (AB) was examined. The results (see green curve in Fig. 4c) demonstrated that substitutional nitrogen impurities induced only a slight asymmetry in the transport between charge carriers at each sides of the Dirac point (as it was observed earlier for boron [73]). Notwithstanding, the carrier mobilities and the conductivities were found to be weakly affected by the dopants, and quantum interference contributions to localization phenomena were found rather marginal. This placed the random incorporation (AB) of nitrogen (boron) atom in graphene as a good solution to dope the material without impeding too much its transport properties.

More recently, the case of an unbalanced sublattice N-doping was investigated [74]. The appearance of a band gap, tunable with the nitrogen concentration, was obtained as a result of the symmetry breaking between the two triangular sublattices of the honeycomb bipartite structure, a fact that was previously predicted for the superlattice model [75,76]. However, here the band gap was found to be robust with respect to a random distribution of the N dopants in only one sublattice (AA). This band gap was even found to persist, while diminished, in the case of an unbalanced sublattice doping, where 20% of the N dopants sit in one sublattice and the remaining 80% N dopants sit in the other sublattice (see Fig. 5a). The opening of a band gap in the graphene electronic spectrum is highly desirable for graphene-based field-effect transistor (GFET) applications since it allows to efficiently turn off the current (see inset of Fig. 5e). Moreover, in the best situation where 100% of the N dopants are placed in only one sublattice, the transport properties at the band edges are found highly asymmetric with outstanding electron transport and poor holes conductive properties (see Fig. 5c and e). This feature, in addition to the creation of a band gap, suggests such unbalanced N-doped graphene systems as an excellent candidate for the development and design of future GFETs. The calculations predict that a nitrogen concentration of at least 4 at.% is required to open a band gap as large as 340 meV, the minimum required for high-speed CMOS FET [77].

In this review, the Kubo–Greenwood approach is applied to the even more particular case of double substitution N-doping, as observed recently by Lv and coworkers [26]. This new study gives results similar to the ones obtained in [74] for a single substitution apart from a small change in the impurity resonant states. The transport properties obtained for all the different N doping configurations discussed above are summarized in Fig. 5. In the left panels of Fig. 5, the DOS, mean free paths and conductivities are plotted versus energy. To get closer to experiment conditions, the right panels of Fig. 5 present the same quantities as a function of gate voltage, assuming the Fermi energy placed in the middle of the gap, or at the Dirac point, and using a gate capacitance of $C_g = 10^{-6}$ F cm^{-2}. The shape of the curves can vary a lot between left and right panels which is due generally to a linear to square root behavior transformation when going from energy to carrier density n (or gate voltage $V_g = ne/C_g$). Moreover, the presence of the gap is somewhat less obvious when plotted as a function of V_g than as a function of the energy. This is because even a small increase in the gate voltage corresponds to an increase of carrier density which is large enough to get away immediately from the band gap region where n vanishes. To get even closer to the experimental set up and be able to draw I–V curves, complementary simulations should be conducted enclosing for instance the full electrostatic environment [78,79] (see Section 7).

As shown in Fig. 4a for 1D nanoribbons, the transport properties are extremely sensitive to impurity resonant states. This is also true in 2D graphene when the concentration of structural defects for instance becomes large enough (usually around 0.5%) to induce energy-dependent resonant peaks in the graphene electronic spectrum, such as illustrated in Figs. 2 and 3. Since, the electronic structure of pristine graphene is symmetric with respect to the Dirac point, the resonant states of structural defects will inevitably prompt asymmetry in the transport characteristics. For instance, the S–T–W defects, having a main resonant peak feature at an energy above the Dirac point, have a drastic impact on electron transport properties (see red curve in Fig. 7). On the opposite side, the 5–8–5 divacancy defects degrade the hole conductivities and mobilities since the resonant peak is located below the Dirac point [64,65]. Therefore, transport measurement can become a complementary spectroscopy technique along with local STS measurements, provided that the concentration of structural defects is large enough, in order to clearly exhibit the energy resonance signatures of defects. This asymmetry in the transport properties could eventually be exploited in logic transistor devices provided a very fine control of the creation of specific types of structural defects.

4. Extended defects

4.1. Grain boundaries

As already illustrated above 2D graphene is found to be heavily affected by structural irregularities. Beyond point defects, covered in the previous section, dislocations and grain boundaries introduce non-local disorder in the hexagonal lattice of graphene. Grain boundaries and dislocations can be characterized by misorientation angles and Burgers vectors, respectively. A systematic way to describe and study grain boundaries and dislocations can be envisioned as a result of introducing a semi-infinite strip of a certain width into an otherwise perfect hexagonal lattice, while keeping the three fold coordination of carbon atoms. Such a description can be formally assigned to a Burgers vector $\vec{b}$ [80].

In general, the transport properties of any system are expected to be degraded by dislocations and grain boundaries. Such a detriment rules out the uniform performance across different individual CVD grown graphene devices, specially as the size of the device is larger than the grain size, thus exhibiting a polycrystalline structure. However, the possibility to identify different grains in graphene by means of TEM has opened the possibility of studying their effect on transport properties [81]. In particular, it has been demonstrated that the connectivity between domains is the crucial factor for the good electrical performance of graphene [82]. By means of a Kubo–Greenwood approach, a recent theoretical investigation has addressed the conductive performance across such polycrystalline graphene further supporting the key issue of the connectivity between domains [83]. Indeed, a bad domain connectivity, referred to as *broken boundaries* in Ref. [83], is found to induce a noticeable increase of the density of states at the charge neutrality point together with low mean free paths and strongly degraded conductivities, a feature similar to the case of amorphous graphene structure that will be discussed later. In the same study, the transport properties are predicted to scale linearly with the grain size for non-broken GBs. Finally, the disorder scattering strength in these polycrystalline graphene structures has been correlated to local fluctuations of the charge inducing self-doping effects (short range electron–hole puddles) in the vicinity of the GBs.

Atomic resolution STM studies of GB in graphite have often been interpreted as consisting of heptagonal and pentagonal defects [84]. Gunlycke and White [85] investigated the transport properties across a specific grain boundary composed of pentagons and octagons [86], showing that grain boundaries could have interesting consequences on the transport properties of graphene. They have analyzed the probability of transmission of charge

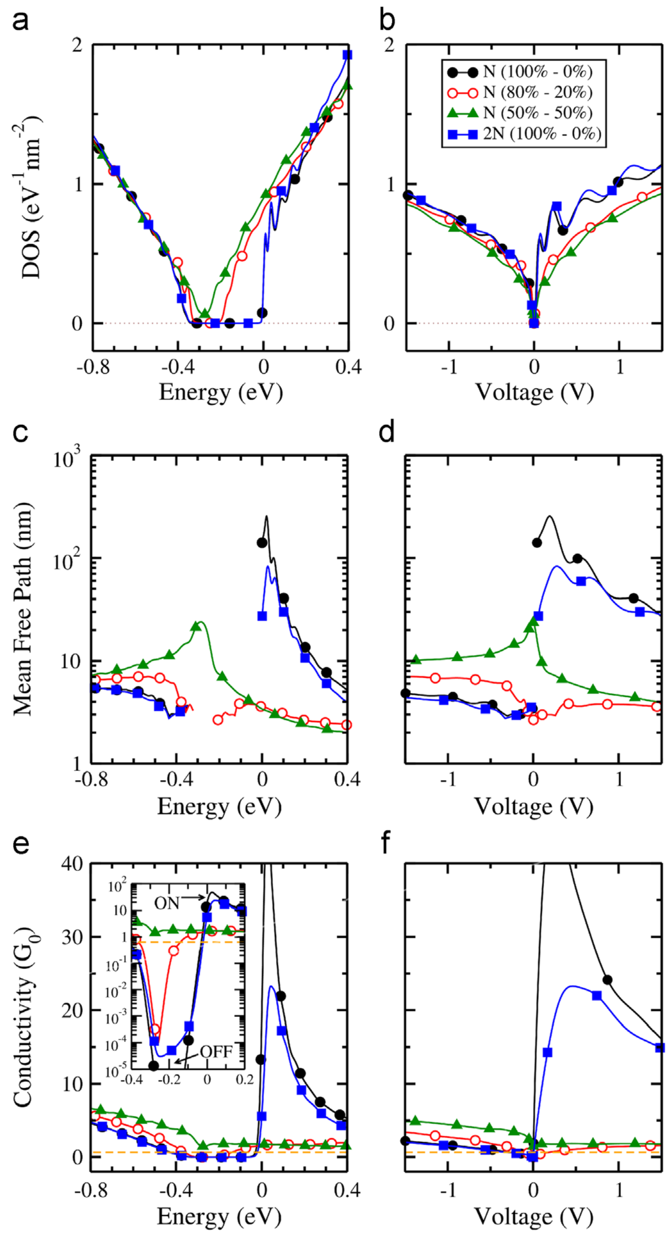

Fig. 5. (Color online) Kubo–Greenwood transport results for various configurations of 4% N-doped graphene i.e. a single N substitution (Fig. 2a) and a double N substitution (2N) (Fig. 2b). For the single N substitution, several sublattice distributions are considered, i.e. 100% of substitutional atoms in sublattice A, 80% of substitutional atoms in sublattice A and 20% of atoms in sublattice B, an homogeneous distribution (50% each). For the double N substitution, only 100% of substitutional atoms in sublattice A are considered. Left panels (a), (c) and (e) present the DOS, mean free paths and semiclassical conductivities, respectively, versus energy, while the right panels (b), (d) and (f) show these quantities versus gate voltage for a gate capacitance $C_g = 10^{-6}$ F cm^{-2}.

carriers across the grain boundary using a first nearest neighbor model, and the Dirac Hamiltonian close to the K and K' valleys. They found that electrons and holes can either be transmitted through or reflected by the grain boundary, according to the law of specular reflection. The probability of transmission depends on the valley degree of freedom, and the angle of incidence (related to the momentum) with respect to the grain boundary [85]. An asymmetry between holes and electrons occurs at each valley, and it is due to the fact that the overall structure is no longer bipartite, since the atoms at the pentagons of the grain boundary cannot be divided into any of the two sublattices.

4.2. Extended lines of defects

As a special case of grain boundaries, extended lines of defects (ELD) can be considered as topological defects introduced in a controlled and ordered manner. In other words, they can be seen as a periodic one dimensional structural irregularities. Using this topological concept, one can imagine to merge two graphene regions with very specific orientations. For instance, an armchair and a zigzag region could be joined by a row of heptagon and pentagons [87]. While apparently hypothetical, a bottom-up approach has been used to create an extended line of defects between two halves of graphene with a relative displacement of $a/2$ between them [86]. In this experiment, two graphene half-sheets were epitaxially grown on a nickel substrate following two different arrangements, inducing an atomic translation relative to each other. Due to this incommensurate scenario, when the two halves merge at the boundary, they are naturally reconstructed through topological defects. The authors suggested that the fingerprints observed in their STM images are caused by an array of defects containing octagonal and pentagonal carbon rings embedded in a graphene sheet. Indeed, STM simulations demonstrate that the lines of defects are constituted by octagons and pentagons. As mentioned above, a 5–8–5 defect is observed as a divacancy reconstruction. However, there are other types of divacancy reconstruction, and thus, different kinds of extended lines of defects can be proposed [88]. For instance, Fig. 6 shows an ELD resulting from the reconstruction of divacancies into t5t7 defects. In general, these one dimensional lines of defects in graphene exhibit localized states along the line and behave like metallic wires embedded in graphene sheets (see Fig. 6). These localized states exhibit a fingerprint on the STM images, and are particular to the specific atomic arrangement of the ELD. This influences its electronic and transport properties. In addition, the localized states which could enhance the chemical reactivity of graphene, thus opening the possibility of arranging molecules or atoms in a linear fashion, acting as a 1D template. In addition, similar to zigzag edges in graphene nanoribbons, they can exhibit spin-polarized states [87,88].

5. Highly defective and amorphous graphene

Structural defects in graphene can be intentionally created and controlled using ion or electron irradiation. By tuning the exposure time and the dose of irradiation it is therefore possible to introduce a huge number of structural defects without destroying the graphene layer via carbon atom sputtering. In 2011, using a HRTEM, Kotakoski and coworkers exposed a suspended graphene membrane to high doses of 100 keV electrons [89]. Instead of collapsing into a 3D amorphous carbon object, they observed the formation of a 2D amorphous graphene layer exhibiting a zoo of structural defects. Amorphous systems are a class of solids where the crystalline structural order is rapidly lost after one or few interatomic distances, and can be seen as an ultimate case of highly structurally defective systems. Such amorphous graphene structures have sparked out a growing attention recently [90–95]. The first theoretical studies on amorphous graphene have predicted a large increase of the density of states at the Dirac point [90–93] (see Fig. 7b), suggesting a semimetal–metal transition from the electronic structure point of view. However, the various transport calculations have drawn two scenario for these amorphous graphene structures. On one hand, the increase of DOS is interpreted as an increase of transmission channels allowing improvements of the transport characteristic of graphene (metallic transport) [92]. On the other hand, the increase of DOS is understood as the superposition of localized states [90] inducing strong scattering events leading to an insulating transport phase, more particularly at low temperature where the contribution of quantum interferences is expected to induce a strong localized transport regime [93]. The key element which could be determinant

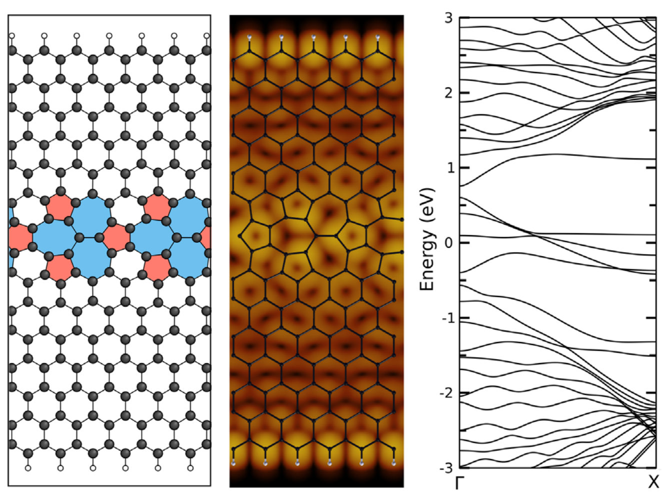

Fig. 6. (Color online) Modeling extended defects in graphene: schematic model (left panel) and simulated STM image (middle panel) of a t5t7 extended line of defects. The electronic structure of the extended line of defects embedded into a ca. 3 nm width nanoribbon is presented in the right panel.

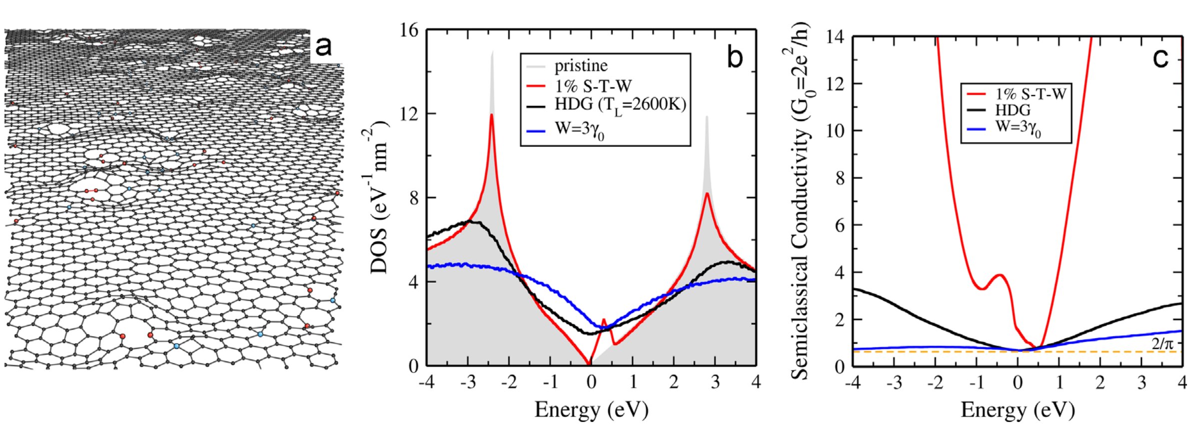

Fig. 7. (Color online) (a) Artistic view of a piece of highly defective graphene (HDG) sample. (b) Density of states (DOS) of a pristine graphene, a HDG layer, a graphene sample with 1% of S–T–W defects, and a strongly disordered graphene system (Andreson disorder $W = 3\gamma_0$). (c) Corresponding semiclassical conductivities of each defective graphene system.

and responsible for these two opposite conclusions on transport is the degree of coalescence and interplay between the localized states induced by each structural defect. If percolation is admitted, then various transmission channels can be created thus allowing carrying electrons. While, if the overlap is small and the hopping between localized states is inefficient then an insulating phase develops.

In a recent study, the transport properties of a highly defective graphene systems were investigated [96]. In contrast to amorphous graphene, a highly defective graphene (HDG) system exhibit both regions of high structural disorder and reconstructed pristine honeycomb lattice area. This realistic model is expected to be close to the experiment in which the carbon network exhibits such a quasi-amorphous structure and thus can share clean and defective domains. The Kubo–Greenwood transport calculations in HDG predicted a non-zero semiclassical conductivity (σ_{sc}), although strongly reduced, i.e. in the range of the semiclassical lower limit of $\sigma_{sc}^{min} = 4e^2/\pi h$, and thus still well below the semiclassical conductivities predicted for highly doped graphene or for graphene with an important concentration of structural defects such as 1% of S–T–W defects (see Fig. 7c). Moreover, particularly short mean free path (below 1 nm) is predicted for such HDG systems, suggesting strong scattering events. At 0 K and in the coherent transport regime, severe contributions of quantum interferences are also observed driving the system to an Anderson insulating phase. Comparisons of transport properties in HDG with a graphene subjected to a well-known *tight-binding* Anderson random disorder model demonstrated that such HDG should actually behave as a Anderson-type 2D insulator, offering thus a genuine playground for exploration of 2D Anderson insulator theories.

6. Conclusion

In summary, the present review reports on the basics of electronic and quantum transport properties in doped and defective graphene. Various types of impurities (dopants, structural defects, extended lines of defects, and highly defective domains) have been considered, and their specific effects on both the electronic structures and the transport properties have been computed. For each defective and doped graphene-based system, a tight-binding model enriched by *ab initio* simulations has been constructed to describe its corresponding electronic behavior. Both the Landauer–Büttiker and the Kubo–Greenwood approaches, which are very complementary methods, have been widely used to investigate the different aspects and transport regimes in defective and doped graphene.

To conclude, because of its remarkable electronic and structural properties, graphene is expected to play an outstanding role in future nanoscale electronics. The complete understanding of fundamental electronic and transport concepts in graphene-based nanomaterials definitely needs for theoretical modeling and advanced quantum simulation, together with joint studies with experiments. Since graphene has still not revealed all its secrets, numerical simulations have still good days to come in predicting new interesting sp^2 carbon topologies and their corresponding electronic behaviors, thus discussing theoretically their potential impact in carbon nanoscience.

7. Methods

7.1. Ab initio

First-principles techniques, commonly referred to as *ab initio* calculations since no input parameters are *a priori* required, are nowadays routinely employed to investigate electronic properties of materials. In the present review, the results obtained from first-principle techniques are restricted to density functional theory (DFT).

The first-principles DFT calculations presented here have been performed using the SIESTA package [97] in the generalized gradient approximation for the exchange-correlation functional in the Perdew–Burke–Ernzerhof (PBE) form [98], with the PBEsol parametrization [99]. Troullier–Martins pseudopotentials are used to account for the core electrons [100]. The valence electron wave functions are expanded in a double-ζ polarized basis set of finite-range numerical pseudoatomic orbitals [101].

Ab initio calculations of defective or doped graphene systems are carried out within the supercell approach which implies periodic repetitions of the simulation box in each direction. To ensure that periodic images of the point defects do not interact with the inner cell, sufficiently large supercells are employed (e.g. 10×10).

7.2. Tight-binding

The *tight-binding* formalism is an approximated approach to describe electronic structure of solids. It consists in expanding the electronic wave functions on a set of atomic orbitals localized on each atomic site. The Hamiltonian of the system is composed of onsite and hopping terms. On its diagonal, the onsite energy terms describe mostly the chemical nature of the atomic sites, while the off-diagonal hopping terms determine the strength of the bonding with neighboring atomic sites. In non-orthogonal *tight-binding* (TB) models, the onsite and hopping terms are accompanied with a third kind of term which allows to build an overlap matrix. All these Hamiltonian (and overlap) matrix elements are parameters which can be fitted to reproduce *ab initio* or experimental band structures. Using the TB parametrization allows to deal with sparse matrix Hamiltonian and therefore investigates electronic structure of large systems containing up to few millions of atoms.

In this review, an orthogonal 3rd nearest neighbors π–π^* TB model enriched by *ab initio* calculations has been used to describe graphene electronic structure. The tight-binding parameters for the pristine graphene are $\varepsilon_{p_z} = 0.59745$ eV for the p_z orbital onsite term, and $\gamma_0^1 = -3.09330$ eV, $\gamma_0^2 = 0.19915$ eV, $\gamma_0^3 = -0.16214$ eV for the 1st, 2nd and 3rd nearest neighbors hopping terms, respectively.

7.3. Landauer–Büttiker

At very short length scales, the semi-classical Boltzmann transport equations fail, because the quantum properties of electrons, such as quantization of the electronic charge, or the phase coherent propagation of the electrons play an important role. The approach proposed by Landauer and Büttiker addresses the quantum nature of the electron with a particular view on transport phenomena as the probability of transmission [102]. Within this framework, a channel of finite length is placed in between semi-infinite contacts. In practice, the quantum conductance of the central channel is inferred from the probability of transmission which is computed using the Landauer formalism, and the surface Green's function matching method, after extracting the first-principles Hamiltonian and overlap matrices [103,104].

7.4. Kubo–Greenwood

As an alternative to overcome the limitations of the semi-classical Boltzmann transport equations, Kubo proposed an exact quantum formulation of the conductivity based on linear response theory [105], suitable for studying strongly disordered systems and complex electron scattering processes with associated mean free paths of the order of the lattice parameter. Greenwood reformulated the original Kubo formula to obtain a simplified and more convenient version [106], the so-called Kubo–Greenwood conductivity formula. The

Kubo–Greenwood formula has been so far widely used to calculate the transport properties in solids.

A real-space order-N Kubo–Greenwood transport approach [107–112] is employed in this review. This approach has already been applied successfully in many studies of transport simulations including various forms of carbon-based materials [73,113–118]. This efficient implementation of the Kubo–Greenwood approach allows the estimation of the main transport quantities in the semi-classical regime (elastic mean free path ℓ_e, conductivity σ_{sc}, and mobility μ) as well as in the quantum regime (localization length ξ). These quantities are extracted from the wave packet propagation dynamics which is monitored by the energy and time-dependent diffusivity $D(E,t) = \Delta R^2(E,t)/t$ where ΔR^2 is the mean quadratic spreading of wave packets.

7.5. Approximations and limitations

Although the approaches employed are very efficient for simulations of electronic transport, they come with approximations and limitations. First, it is interesting to note that DFT is deficient in predicting good band gaps and usually underestimate their values. More accurate techniques exist, such as *GW* corrections, but the price to pay is an important increase of computational power. In this review, only few cases are concerned since most of the time, defective and doped graphene-based systems do not exhibit a band gap.

Then, during the TB parametrization of the electronic structure, some information and precision are inevitably lost compared to the initial DFT calculation. The accuracy of the TB models reside in the number of atomic orbitals considered on each site, and the range used in the description of nearest neighbor interactions.

The transport approaches used in this review also have some limitations. An electrostatic environment, such as the presence of a gate oxide, has not been taken into account and neither the screening effects [79].

The Kubo–Greenwood method being a *bulk* approach, the system is considered as virtually infinite. In practice, periodic boundary conditions are applied meaning that the presence of contacts is not taken into account. The Kubo–Greenwood approach describes the *bulk*, or equivalently the *intrinsic*, transport properties. Hence, the Kubo–Greenwood approach is rather not appropriate to describe ballistic transport but well suited to study diffusive and localization transport regime.

As opposed to the Kubo–Greenwood, the Landauer–Büttiker approach does address the effect of contacts by considering semi-infinite open leads. However in practice, the leads correspond to ideal contacts, here pristine graphene nanoribbons of the same width as of the central channel ribbon. In any experiment, the contacts are much less ideal and current injection can be strongly reduced. Finally, the out-of-equilibrium transport regime has not been considered in this review. On the contrary we studied only the (near) equilibrium regime where response of the materials is linear with the applied field. Saturation effects are for instance not accessible.

Acknowledgments

The authors thank H. Amara, X. Declerck, S. M.-M. Dubois, N. Leconte, F. Varchon, Z. Zanolli, and B. Zheng for their contributions and constructive discussions as former members of the IMCN-NAPS group. J.-C.C., A.L. and A.R.B.-M. acknowledge financial support from FNRS of Belgium. This research is connected to the ARC Graphene Nano-electromechanics (No. 11/16-037) and to the ICT FET Flagship on Graphene entitled "*Graphene-based revolutions in ICT and beyond*". Computational resources are provided by the UCL-CISM.

References

[1] P. Debye, P. Scherrer, Physikalische Zeitschrift 18 (1917) 291–301.
[2] A.W. Hull, Physical Review 10 (6) (1917) 661–696, http://dx.doi.org/10.1103/PhysRev.10.661.
[3] J.D. Bernal, Proceedings of the Royal Society of London. Series A 106 (740) (1924) 749–773, http://dx.doi.org/10.1098/rspa.1924.0101.
[4] R.E. Franklin, Acta Crystallographica 3 (2) (1950) 107–121, http://dx.doi.org/10.1107/S0365110X50000264.
[5] M. Dresselhaus, G. Dresselhaus, Advances in Physics 30 (2) (1981) 139–326, http://dx.doi.org/10.1080/00018738100101367.
[6] A.H. Castro Neto, F. Guinea, N.M.R. Peres, K.S. Novoselov, A.K. Geim, Reviews of Modern Physics 81 (1) (2009) 109–162, http://dx.doi.org/10.1103/RevModPhys.81.109.
[7] N.M.R. Peres, Reviews of Modern Physics 82 (3) (2010) 2673–2700, http://dx.doi.org/10.1103/RevModPhys.82.2673.
[8] W. Zhao, O. Höfert, K. Gotterbarm, J. Zhu, C. Papp, H.-P. Steinrück, The Journal of Physical Chemistry C 116 (8) (2012) 5062–5066, http://dx.doi.org/10.1021/jp209927m.
[9] S.H. Rhim, Y. Qi, Y. Liu, M. Weinert, L. Li, Applied Physics Letters 100 (23) (2012), http://dx.doi.org/10.1063/1.4726281 233119.
[10] C.D. Wang, M.F. Yuen, T.W. Ng, S.K. Jha, Z.Z. Lu, S.Y. Kwok, T.L. Wong, X. Yang, C.S. Lee, S.T. Lee, W.J. Zhang, Applied Physics Letters 100 (25) (2012), http://dx.doi.org/10.1063/1.4729823 253107.
[11] Y. Xue, B. Wu, L. Jiang, Y. Guo, L. Huang, J. Chen, J. Tan, D. Geng, B. Luo, W. Hu, G. Yu, Y. Liu, Journal of the American Chemical Society 134 (27) (2012) 11060–11063, http://dx.doi.org/10.1021/ja302483t.
[12] H. Gao, L. Song, W. Guo, L. Huang, D. Yang, F. Wang, Y. Zuo, X. Fan, Z. Liu, W. Gao, R. Vajtai, K. Hackenberg, P.M. Ajayan, Carbon 50 (12) (2012) 4476–4482, http://dx.doi.org/10.1016/j.carbon.2012.05.026.
[13] R.J. Koch, M. Weser, W. Zhao, F. Viñes, K. Gotterbarm, S.M. Kozlov, O. Höfert, M. Ostler, C. Papp, J. Gebhardt, H.-P. Steinrück, A. Görling, T. Seyller, Physical Review B 86 (7) (2012) 075401, http://dx.doi.org/10.1103/PhysRevB.86.075401.
[14] E. Velez-Fort, C. Mathieu, E. Pallecchi, M. Pigneur, M.G. Silly, R. Belkhou, M. Marangolo, A. Shukla, F. Sirotti, A. Ouerghi, ACS Nano 6 (12) (2012) 10893–10900, doi:http://dx.doi.org/10.1021/nn304315z.
[15] K. Brenner, R. Murali, Applied Physics Letters 98 (11) (2011), http://dx.doi.org/10.1063/1.3562018 113115.
[16] Z. Jin, J. Yao, C. Kittrell, J.M. Tour, ACS Nano 5 (5) (2011) 4112–4117, http://dx.doi.org/10.1021/nn200766e.
[17] G. Imamura, K. Saiki, The Journal of Physical Chemistry C 115 (20) (2011) 10000–10005, http://dx.doi.org/10.1021/jp202128f.
[18] L. Zhao, R. He, K.T. Rim, T. Schiros, K.S. Kim, H. Zhou, C. Gutiérrez, S.P. Chockalingam, C.J. Arguello, L. Pálová, D. Nordlund, M.S. Hybertsen, D.R. Reichman, T.F. Heinz, P. Kim, A. Pinczuk, G.W. Flynn, A.N. Pasupathy, Science 333 (6045) (2011) 999–1003, http://dx.doi.org/10.1126/science.1208759.
[19] D. Usachov, O. Vilkov, A. Grüneis, D. Haberer, A. Fedorov, V.K. Adamchuk, A.B. Preobrajenski, P. Dudin, A. Barinov, M. Oehzelt, C. Laubschat, D.V. Vyalikh, Nano Letters 11 (12) (2011) 5401–5407, http://dx.doi.org/10.1021/nl2031037.
[20] X. Wang, X. Li, L. Zhang, Y. Yoon, P.K. Weber, H. Wang, J. Guo, H. Dai, Science 324 (5928) (2009) 768–771, http://dx.doi.org/10.1126/science.1170335.
[21] N. Li, Z. Wang, K. Zhao, Z. Shi, Z. Gu, S. Xu, Carbon 48 (1) (2010) 255–259, http://dx.doi.org/10.1016/j.carbon.2009.09.013.
[22] Y.-C. Lin, C.-Y. Lin, P.-W. Chiu, Applied Physics Letters 96 (13) (2010), http://dx.doi.org/10.1063/1.3368697 133110.
[23] J. Gebhardt, R.J. Koch, W. Zhao, O. Höfert, K. Gotterbarm, S. Mammadov, C. Papp, A. Görling, H.-P. Steinrück, T. Seyller, Growth and Electronic Structure of Boron-Doped Graphene, ArXiv/1212.0212.
[24] Y.A. Kim, K. Fujisawa, H. Muramatsu, T. Hayashi, M. Endo, T. Fujimori, K. Kaneko, M. Terrones, J. Behrends, A. Eckmann, C. Casiraghi, K.S. Novoselov, R. Saito, M.S. Dresselhaus, ACS Nano 6 (7) (2012) 6293–6300, http://dx.doi.org/10.1021/nn301728j.
[25] Y.-B. Tang, L.-C. Yin, Y. Yang, X.-H. Bo, Y.-L. Cao, H.-E. Wang, W.-J. Zhang, I. Bello, S.-T. Lee, H.-M. Cheng, C.-S. Lee, ACS Nano 6 (3) (2012) 1970–1978, http://dx.doi.org/10.1021/nn3005262.
[26] R. Lv, Q. Li, A.R. Botello-Méndez, T. Hayashi, B. Wang, A. Berkdemir, Q. Hao, A. L. Elías, R. Cruz-Silva, H.R. Gutiérrez, Y.A. Kim, H. Muramatsu, J. Zhu, M. Endo, H. Terrones, J.-C. Charlier, M. Pan, M. Terrones, Scientific Reports 2 (2012) 586, http://dx.doi.org/10.1038/srep00586.
[27] Z.-S. Wu, S. Yang, Y. Sun, K. Parvez, X. Feng, K. Müllen, Journal of the American Chemical Society 134 (22) (2012) 9082–9085, http://dx.doi.org/10.1021/ja3030565.
[28] G. Wu, N.H. Mack, W. Gao, S. Ma, R. Zhong, J. Han, J.K. Baldwin, P. Zelenay, ACS Nano 6 (11) (2012) 9764–9776, http://dx.doi.org/10.1021/nn303275d.
[29] K. Parvez, S. Yang, Y. Hernandez, A. Winter, A. Turchanin, X. Feng, K. Müllen, ACS Nano 6 (11) (2012) 9541–9550, http://dx.doi.org/10.1021/nn302674k.
[30] Z.-H. Sheng, L. Shao, J.-J. Chen, W.-J. Bao, F.-B. Wang, X.-H. Xia, ACS Nano 5 (6) (2011) 4350–4358, http://dx.doi.org/10.1021/nn103584t.
[31] I.-Y. Jeon, D. Yu, S.-Y. Bae, H.-J. Choi, D.W. Chang, L. Dai, J.-B. Baek, Chemistry of Materials 23 (17) (2011) 3987–3992, http://dx.doi.org/10.1021/cm201542m.
[32] L. Feng, Y. Chen, L. Chen, ACS Nano 5 (12) (2011) 9611–9618, http://dx.doi.org/10.1021/nn202906f.
[33] L. Qu, Y. Liu, J.-B. Baek, L. Dai, ACS Nano 4 (3) (2010) 1321–1326, http://dx.doi.org/10.1021/nn901850u.

[34] Y. Feng, F. Li, Z. Hu, X. Luo, L. Zhang, X.-F. Zhou, H.-T. Wang, J.-J. Xu, E.G. Wang, Physical Review B 85 (15) (2012) 155454, http://dx.doi.org/10.1103/PhysRevB.85.155454.
[35] B. Xiong, Y. Zhou, Y. Zhao, J. Wang, X. Chen, R. O'Hayre, Z. Shao, Carbon 52 (0) (2013) 181–192, http://dx.doi.org/10.1016/j.carbon.2012.09.019.
[36] N. Soin, S. Sinha Roy, S. Roy, K.S. Hazra, D.S. Misra, T.H. Lim, C.J. Hetherington, J.A. McLaughlin, The Journal of Physical Chemistry C 115 (13) (2011) 5366–5372, http://dx.doi.org/10.1021/jp110476m.
[37] U.A. Palnitkar, R.V. Kashid, M.A. More, D.S. Joag, L.S. Panchakarla, C.N.R. Rao, Applied Physics Letters 97 (6) (2010), http://dx.doi.org/10.1063/1.3464168 063102.
[38] H.M. Jeong, J.W. Lee, W.H. Shin, Y.J. Choi, H.J. Shin, J.K. Kang, J.W. Choi, Nano Letters 11 (6) (2011) 2472–2477, http://dx.doi.org/10.1021/nl2009058.
[39] Z.M. Ao, A.D. Hernández-Nieves, F.M. Peeters, S. Li, Physical Chemistry Chemical Physics 14 (4) (2012) 1463–1467, http://dx.doi.org/10.1039/C1CP23153G.
[40] O.S. Kwon, S.J. Park, J.-Y. Hong, A.-R. Han, J.S. Lee, J.S. Lee, J.H. Oh, J. Jang, ACS Nano 6 (2) (2012) 1486–1493, http://dx.doi.org/10.1021/nn204395n.
[41] Y. Wang, Y. Shao, D.W. Matson, J. Li, Y. Lin, ACS Nano 4 (4) (2010) 1790–1798, http://dx.doi.org/10.1021/nn100315s.
[42] A.L.M. Reddy, A. Srivastava, S.R. Gowda, H. Gullapalli, M. Dubey, P.M. Ajayan, ACS Nano 4 (11) (2010) 6337–6342, http://dx.doi.org/10.1021/nn101926g.
[43] C.-S. Liu, Z. Zeng, Applied Physics Letters 96 (12) (2010), http://dx.doi.org/10.1063/1.3367773 123101.
[44] Y. Jeong, T.M. Chung, Carbon 49 (1) (2011) 140–146, http://dx.doi.org/10.1016/j.carbon.2010.08.053.
[45] F. Joucken, Y. Tison, J. Lagoute, J. Dumont, D. Cabosart, B. Zheng, V. Repain, C. Chacon, Y. Girard, A.R. Botello-Méndez, S. Rousset, R. Sporken, J.-C. Charlier, L. Henrard, Physical Review B 85 (16) (2012) 161408, http://dx.doi.org/10.1103/PhysRevB.85.161408.
[46] P. Lambin, H. Amara, F. Ducastelle, L. Henrard, Physical Review B 86 (4) (2012) 045448, http://dx.doi.org/10.1103/PhysRevB.86.045448.
[47] J. Tersoff, D.R. Hamann, Physical Review Letters 50 (25) (1983) 1998–2001, http://dx.doi.org/10.1103/PhysRevLett.50.1998.
[48] B. Zheng, P. Hermet, L. Henrard, ACS Nano 4 (7) (2010) 4165–4173, http://dx.doi.org/10.1021/nn1002425.
[49] E. Cockayne, Physical Review B 85 (12) (2012) 125409, http://dx.doi.org/10.1103/PhysRevB.85.125409.
[50] H. Terrones, A. Mackay, Carbon 30 (8) (1992) 1251–1260, http://dx.doi.org/10.1016/0008-6223(92)90066-6.
[51] M. Terrones, H. Terrones, Fullerene Science and Technology 4 (3) (1996) 517–533, http://dx.doi.org/10.1080/10641229608001568.
[52] P.A. Thrower, Chemistry and Physics of Carbon 5 (1969) 217–230.
[53] A. Stone, D. Wales, Chemical Physics Letters 128 (5–6) (1986) 501–503, http://dx.doi.org/10.1016/0009-2614(86)80661-3.
[54] V.H. Crespi, L.X. Benedict, M.L. Cohen, S.G. Louie, Physical Review B 53 (1996) R13303–R13305, http://dx.doi.org/10.1103/PhysRevB.53.R13303.
[55] H. Terrones, M. Terrones, E. Hernández, N. Grobert, J.-C. Charlier, P.M. Ajayan, Physical Review Letters 84 (8) (2000) 1716–1719, http://dx.doi.org/10.1103/PhysRevLett.84.1716.
[56] A. Krasheninnikov, P. Lehtinen, A. Foster, R. Nieminen, Chemical Physics Letters 418 (1–3) (2006) 132–136, http://dx.doi.org/10.1016/j.cplett.2005.10.106.
[57] M.M. Ugeda, D. Fernández-Torre, I. Brihuega, P. Pou, A.J. Martínez-Galera, R. Pérez, J.M. Gómez-Rodríguez, Physical Review Letters 107 (11) (2011) 116803, http://dx.doi.org/10.1103/PhysRevLett.107.116803.
[58] J.-H. Chen, W.G. Cullen, C. Jang, M.S. Fuhrer, E.D. Williams, Physical Review Letters 102 (23) (2009) 236805, http://dx.doi.org/10.1103/PhysRevLett.102.236805.
[59] B.R.K. Nanda, M. Sherafati, Z.S. Popović, S. Satpathy, New Journal of Physics 14 (8) (2012) 083004, http://dx.doi.org/10.1088/1367-2630/14/8/083004.
[60] A. Cresti, F. Ortmann, T. Louvet, D. Van Tuan, S. Roche, Physical Review Letters 110 (19) (2013) 196601, http://dx.doi.org/10.1103/PhysRevLett.110.196601.
[61] F. Ducastelle, Physical Review B 88 (7) (2013) 075413, http://dx.doi.org/10.1103/PhysRevB.88.075413.
[62] J.-H. Chen, L. Li, W.G. Cullen, E.D. Williams, M.S. Fuhrer, Nature Physics 7 (7) (2011) 535–538, http://dx.doi.org/10.1038/nphys1962.
[63] F. Banhart, J. Kotakoski, A.V. Krasheninnikov, ACS Nano 5 (1) (2010) 26–41, http://dx.doi.org/10.1021/nn102598m.
[64] A. Lherbier, S.M.-M. Dubois, X. Declerck, S. Roche, Y.-M. Niquet, J.-C. Charlier, Physical Review Letters 106 (2011) 046803, http://dx.doi.org/10.1103/PhysRevLett.106.046803.
[65] A. Lherbier, S.M.-M. Dubois, X. Declerck, Y.-M. Niquet, S. Roche, J.-C. Charlier, Physical Review B 86 (7) (2012) 075402, http://dx.doi.org/10.1103/PhysRevB.86.075402.
[66] H. Amara, S. Latil, V. Meunier, P. Lambin, J.-C. Charlier, Physical Review B 76 (11) (2007) 115423, http://dx.doi.org/10.1103/PhysRevB.76.115423.
[67] M.M. Ugeda, I. Brihuega, F. Hiebel, P. Mallet, J.-Y. Veuillen, J.M. Gómez-Rodríguez, F. Ynduráin, Physical Review B 85 (12) (2012) 121402, http://dx.doi.org/10.1103/PhysRevB.85.121402.
[68] H. Terrones, R. Lv, M. Terrones, M.S. Dresselhaus, Reports on Progress in Physics 75 (6) (2012) 062501, http://dx.doi.org/10.1088/0034-4885/75/6/062501.
[69] S.M.-M. Dubois, Z. Zanolli, X. Declerck, J.-C. Charlier, European Physical Journal B 72 (1) (2009) 1–24, http://dx.doi.org/10.1140/epjb/e2009-00327-8.
[70] B. Biel, X. Blase, F. Triozon, S. Roche, Physical Review Letters 102 (9) (2009) 096803, http://dx.doi.org/10.1103/PhysRevLett.102.096803.
[71] E. Cruz-Silva, Z.M. Barnett, B.G. Sumpter, V. Meunier, Physical Review B 83 (15) (2011) 155445, http://dx.doi.org/10.1103/PhysRevB.83.155445.
[72] B. Biel, A. Cresti, R. Avriller, S. Dubois, A. López-Bezanilla, F. Triozon, X. Blase, J.-C. Charlier, S. Roche, Physica Status Solidi C 7 (11–12) (2010) 2628–2631, http://dx.doi.org/10.1002/pssc.200983826.
[73] A. Lherbier, X. Blase, Y.-M. Niquet, F. Triozon, S. Roche, Physical Review Letters 101 (3) (2008) 036808, http://dx.doi.org/10.1103/PhysRevLett.101.036808.
[74] A. Lherbier, A.R. Botello-Méndez, J.-C. Charlier, Nano Letters 13 (4) (2013) 1446–1450, http://dx.doi.org/10.1021/nl304351z.
[75] R. Martinazzo, S. Casolo, G.F. Tantardini, Physical Review B 81 (2010) 245420, http://dx.doi.org/10.1103/PhysRevB.81.245420.
[76] S. Casolo, R. Martinazzo, G.F. Tantardini, The Journal of Physical Chemistry C 115 (8) (2011) 3250–3256, http://dx.doi.org/10.1021/jp109741s arXiv:http://pubs.acs.org/doi/pdf/10.1021/jp109741s.
[77] K. Kim, J.-Y. Choi, T. Kim, S.-H. Cho, H.-J. Chung, Nature 479 (7373) (2011) 338–344, http://dx.doi.org/10.1038/nature10680.
[78] V.H. Nguyen, F. Mazzamuto, J. Saint-Martin, A. Bournel, P. Dollfus, Nanotechnology 23 (6) (2012) 065201, http://dx.doi.org/10.1088/0957-4484/23/6/065201.
[79] P. Marconcini, A. Cresti, F. Triozon, G. Fiori, B. Biel, Y.-M. Niquet, M. Macucci, S. Roche, ACS Nano 6 (9) (2012) 7942–7947, http://dx.doi.org/10.1021/nn3024046.
[80] O.V. Yazyev, S.G. Louie, Physical Review B 81 (19) (2010) 195420, http://dx.doi.org/10.1103/PhysRevB.81.195420.
[81] P.Y. Huang, C.S. Ruiz-Vargas, A.M.v.d. Zande, W.S. Whitney, M.P. Levendorf, J.W. Kevek, S. Garg, J.S. Alden, C.J. Hustedt, Y. Zhu, J. Park, P.L. McEuen, D.A. Muller, Nature 469 (7330) (2011) 389–392, http://dx.doi.org/10.1038/nature09718.
[82] A.W. Tsen, L. Brown, M.P. Levendorf, F. Ghahari, P.Y. Huang, R.W. Havener, C.S. Ruiz-Vargas, D.A. Muller, P. Kim, J. Park, Science 336 (6085) (2012) 1143–1146, http://dx.doi.org/10.1126/science.1218948.
[83] D. Van Tuan, J. Kotakoski, T. Louvet, F. Ortmann, J.C. Meyer, S. Roche, Nano Letters 13 (4) (2013) 1730–1735, http://dx.doi.org/10.1021/nl400321r arXiv:http://pubs.acs.org/doi/pdf/10.1021/nl400321r.
[84] P. Simonis, C. Goffaux, P. Thiry, L. Biro, P. Lambin, V. Meunier, Surface Science 511 (1–3) (2002) 319–322, http://dx.doi.org/10.1016/S0039-6028(02)01511-X.
[85] D. Gunlycke, C.T. White, Physical Review Letters 106 (13) (2011) 136806, http://dx.doi.org/10.1103/PhysRevLett.106.136806.
[86] J. Lahiri, Y. Lin, P. Bozkurt, I.I. Oleynik, M. Batzill, Nature 5 (5) (2010) 326–329, http://dx.doi.org/10.1038/nnano.2010.53.
[87] A.R. Botello-Mendez, E. Cruz-Silva, F. Lopez-Urias, B.G. Sumpter, V. Meunier, M. Terrones, H. Terrones, ACS Nano 3 (11) (2009) 3606–3612, http://dx.doi.org/10.1021/nn900614x.
[88] A.R. Botello-Méndez, X. Declerck, M. Terrones, H. Terrones, J.-C. Charlier, Nanoscale 3 (7) (2011) 2868, http://dx.doi.org/10.1039/c0nr00820f.
[89] J. Kotakoski, A.V. Krasheninnikov, U. Kaiser, J.C. Meyer, Physical Review Letters 106 (10) (2011) 105505, http://dx.doi.org/10.1103/PhysRevLett.106.105505.
[90] V. Kapko, D.A. Drabold, M.F. Thorpe, J.C. Meyer, Physica Status Solidi (b) 247 (5) (2010) 1197–1200, http://dx.doi.org/10.1002/pssb.200945581.
[91] Y. Li, F. Inam, A. Kumar, M.F. Thorpe, D.A. Drabold, Physica Status Solidi (b) (9) (2011) 2082–2086, http://dx.doi.org/10.1002/pssb.201147195.
[92] E. Holmström, J. Fransson, O. Eriksson, R. Lizárraga, B. Sanyal, S. Bhandary, M.I. Katsnelson, Physical Review B 84 (2011) 205414, http://dx.doi.org/10.1103/PhysRevB.84.205414.
[93] D. Van Tuan, A. Kumar, S. Roche, F. Ortmann, M.F. Thorpe, P. Ordejon, Physical Review B 86 (2012) 121408, http://dx.doi.org/10.1103/PhysRevB.86.121408.
[94] A. Kumar, M. Wilson, M.F. Thorpe, Journal of Physics: Condensed Matter 24 (48) (2012) 485003.
[95] Y. Li, D.A. Drabold, Physica Status Solidi (b) 250 (5) (2012) 1012–1019. doi:http://dx.doi.org/10.1002/pssb.201248481.
[96] A. Lherbier, S. Roche, O.A. Restrepo, Y.-M. Niquet, A. Delcorte, J.-C. Charlier, Nano Research 6 (5) (2013) 326–334, http://dx.doi.org/10.1007/s12274-013-0309-7.
[97] J.M. Soler, E. Artacho, J.D. Gale, A. García, J. Junquera, P. Ordejón, D. Sánchez-Portal, Journal of Physics: Condensed Matter 14 (11) (2002) 2745.
[98] J.P. Perdew, K. Burke, M. Ernzerhof, Physical Review Letters 77 (1996) 3865–3868, http://dx.doi.org/10.1103/PhysRevLett.77.3865.
[99] J.P. Perdew, A. Ruzsinszky, G.I. Csonka, O.A. Vydrov, G.E. Scuseria, L.A. Constantin, X. Zhou, K. Burke, Physical Review Letters 100 (2008) 136406, http://dx.doi.org/10.1103/PhysRevLett.100.136406.
[100] N. Troullier, J.L. Martins, Physical Review B 43 (1991) 1993–2006, http://dx.doi.org/10.1103/PhysRevB.43.1993.
[101] E. Artacho, D. Sánchez-Portal, P. Ordejón, A. García, J.M. Soler, Physica Status Solidi (b) (1) (1999) 809–817, doi:http://dx.doi.org/10.1002/(SICI)1521-3951(199909)215:1 < 809::AID-PSSB809 > 3.0.CO;2-0.
[102] S. Datta, Electronic Transport in Mesoscopic Systems, Cambridge University Press, 1997.
[103] V. Meunier, B.G. Sumpter, Journal of Chemical Physics 123 (2) (2005) 024705–024708, http://dx.doi.org/10.1063/1.1931547.
[104] E. Cruz-Silva, F. López-Urías, E. Munoz-Sandoval, B.G. Sumpter, H. Terrones, J. Charlier, V. Meunier, M. Terrones, ACS Nano 3 (7) (2009) 1913–1921, http://dx.doi.org/10.1021/nn900286h.
[105] R. Kubo, Journal of the Physical Society of Japan 12 (6) (1957) 570–586, http://dx.doi.org/10.1143/JPSJ.12.570.
[106] D.A. Greenwood, Proceedings of the Physical Society 71 (4) (1958) 585.
[107] D. Mayou, EPL (Europhysics Letters) 6 (6) (1988) 549.

[108] D. Mayou, S.N. Khanna, Journal de Physique I, France 5 (9) (1995) 1199–1211, http://dx.doi.org/10.1051/jp1:1995191.
[109] S. Roche, D. Mayou, Physical Review Letters 79 (1997) 2518–2521, http://dx.doi.org/10.1103/PhysRevLett.79.2518.
[110] S. Roche, Physical Review B 59 (1999) 2284–2291, http://dx.doi.org/10.1103/PhysRevB.59.2284.
[111] F. Triozon, J. Vidal, R. Mosseri, D. Mayou, Physical Review B 65 (2002) 220202, http://dx.doi.org/10.1103/PhysRevB.65.220202.
[112] Z. Fan, A. Uppstu, T. Siro, A. Harju, Efficient Linear Scaling Quantum Transport Calculations on Graphics Processing Units and Applications on Electron Transport in Graphene, arXiv:1307.0288.
[113] S. Roche, F. Triozon, A. Rubio, D. Mayou, Physics Letters A 285 (1–2) (2001) 94–100, http://dx.doi.org/10.1016/S0375-9601(01)00330-9.
[114] S. Latil, S. Roche, D. Mayou, J.-C. Charlier, Physical Review Letters 92 (2004) 256805, http://dx.doi.org/10.1103/PhysRevLett.92.256805.
[115] S. Latil, S. Roche, J.-C. Charlier, Nano Letters 5 (11) (2005) 2216–2219, http://dx.doi.org/10.1021/nl0514386 arXiv:http://pubs.acs.org/doi/pdf/10.1021/nl0514386.
[116] A. Lherbier, B. Biel, Y.-M. Niquet, S. Roche, Physical Review Letters 100 (3) (2008) 036803, http://dx.doi.org/10.1103/PhysRevLett.100.036803.
[117] H. Ishii, F. Triozon, N. Kobayashi, K. Hirose, S. Roche, Comptes Rendus Physique 10 (4) (2009) 283–296, http://dx.doi.org/10.1016/j.crhy.2009.04.003.
[118] S. Roche, N. Leconte, F. Ortmann, A. Lherbier, D. Soriano, J.-C. Charlier, Solid State Communications 152 (15) (2012) 1404–1410, http://dx.doi.org/10.1016/j.ssc.2012.04.030.